

# ESI: Diverse Morphologies in Thin-film Bijels by Varying Film Thickness and Composition<sup>†</sup>

Joseph M. Carmack<sup>\*a</sup> and Paul C. Millett<sup>a</sup>

Received Xth XXXXXXXXXXXX 20XX, Accepted Xth XXXXXXXXXXXX 20XX

First published on the web Xth XXXXXXXXXXXX 200X

DOI: 10.1039/b000000x

## 1 Supplementary Material

### 1.1 Curvature Calculation

To calculate curvatures on a simulated bijel, the data, stored in the Legacy VTK file format, is loaded into paraview. An isosurface filter is then applied for values of  $\phi = 0$  which represents the interface between the two binary phases as mentioned previously. Due to the high density of particles that attach to the bijel interfaces and the random fluctuations in  $\phi_i$  from the thermal noise term in the Cahn-Hilliard equation, the interface has roughness which introduces significant noise into the calculated isosurface. In order to smooth out the isosurface to more accurately represent the bijel interface, the VTK data was downsampled by a factor of six nodes using Paraview's extract subset filter before applying the isosurface filter. Several different downsampling rates were tested and a six node rate was identified as the rate that produced the most accurate match to the real interface. After downsampling, Paraview's curvature filter was applied to the isosurface to calculate both  $K$  and  $H$  at each point on the isosurface. Next, Paraview's threshold filter was applied to filter out any extreme curvature values resulting from remaining artifacts in the isosurface. Any curvatures corresponding to a radius of curvature smaller than the particle's average radius were filtered out in this step. Lastly, the area-averaged curvatures were extracted using the integrate variables filter in Paraview. This entire procedure was scripted in the Python programming language and executed via Paraview's Python interface. Benchmarking in a similar fashion to the work of the Thijssen group<sup>1</sup> was carried out to ensure results were as expected.

The curvature analysis process using Paraview outlined above was benchmarked using periodic gyroid (with  $L =$  unit cell size for the gyroid) and spherical structures to probe the accuracy of the method. The area-averaged Gaussian and Mean curvatures vary with the average domain size of the bijel; Consequently, it is necessary to normalize the curvatures in some way to allow for comparison of morphologies with differing average domain sizes. This is done by normalizing the curvatures with the interface area to volume ratio,  $\Sigma = A/V$ . The normalized curvatures are then given by  $K\Sigma^{-2}$

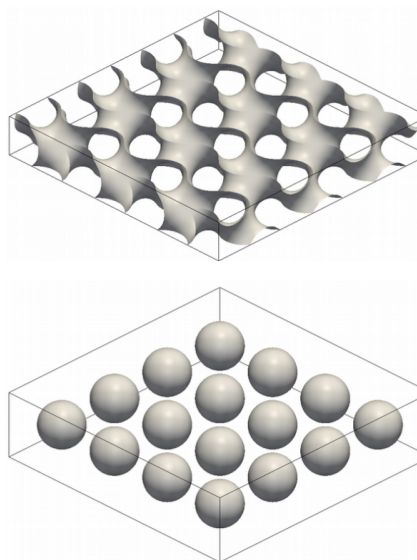


**Fig. 1** Test cases for curvature analysis with the Paraview software suite. Gyroid structure with dimensions  $400 \times 400 \times 60 \delta^3$  and spheres with a diameter of  $20\delta$ . The gyroid structure has  $L = 60\delta$ . Area-averaged curvatures normalized by surface-to-volume ratio and corresponding error for the gyroid structure are  $\langle K \rangle \Sigma^{-2} = -1.8946$ ,  $\epsilon_r = 12.4\%$  and  $\langle H \rangle \Sigma^{-1} = -0.0103$ ,  $\epsilon_a = 1.0\%$ . Area-averaged curvatures normalized by surface-to-volume ratio and corresponding error for the spheres are  $\langle K \rangle \Sigma^{-2} = -2.1673$ ,  $\epsilon_r = 1.55\%$  and  $\langle H \rangle \Sigma^{-1} = 4.6880$ ,  $\epsilon_r = 0.87\%$ .

and  $H\Sigma^{-1}$ . The data presented in the paper is not normalized in this fashion because we found the non-normalized data to be more intuitive and thus easier to interpret.

Spheres and gyroid structures were generated in thin-film geometries as shown in Figure 1. Area-averaged and normalized curvatures were calculated for these topologies and the results compared against their analytical values. Results, including relative and absolute errors, are shown in the caption for Figure 1. Additionally, a test of the curvatures dependence

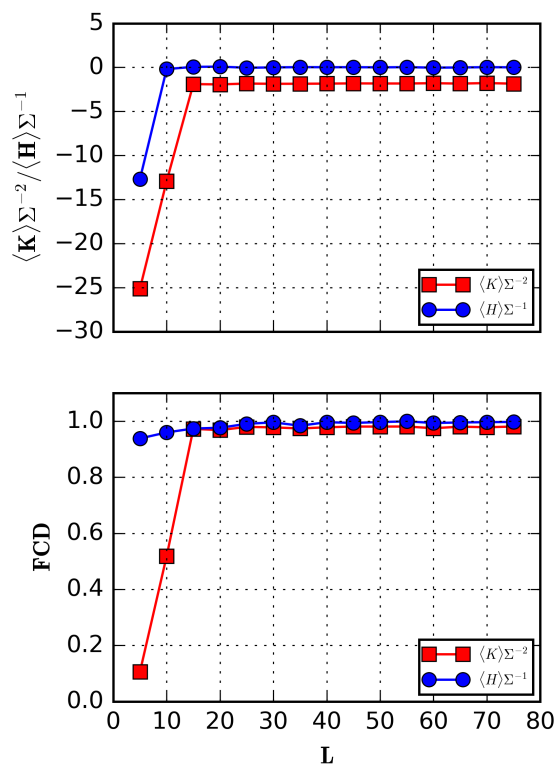


**Fig. 2** The top plot shows the area-averaged curvatures for the gyroid structure as a function of  $L$ . The bottom plot shows the fraction of curvature data ( $FCD$ ) for a given  $L$  used to generate each data point in the top plot. The reason for the fraction being so low for small values of  $L$  is that most of the curvatures calculated are very extreme and are consequently filtered out by the Paraview threshold filter.

on the domain size for the gyroid structures was conducted and results are shown in Figure 2. It was found that significant errors were produced when the domain size of the gyroid is reduced below  $15 \delta$ . This is due to the discreteness of the gyroid data which does not provide enough resolution to accurately capture the gyroid surface. To account for this situation, during the early stages of binary phase separation in our bijel simulations, when domain sizes are very small, curvature calculations were not performed (for the first 10,000 time steps).

## 1.2 Interfacial Particle Coverage

In addition to the fraction of particles attached to the interface, we also tracked the percentage of interfacial area covered by the particles. This was calculated by assuming that the portion of interface covered by a particle was flat and that the particles covered an area equal to their largest cross-sectional area  $A_c = \pi r_p^2$ , where  $r_p$  is the particle radius. This calculation

is therefore not exact and tends to undershoot the true value, more so for thick films because they have a higher ratio of curved to flat interface than the thinner films. Nonetheless, it should still give a good approximation of the actual particle coverage. The percent of the interface covered by particles calculated in this fashion is given in Figures 3 and 4 for thick and thin films, respectively.

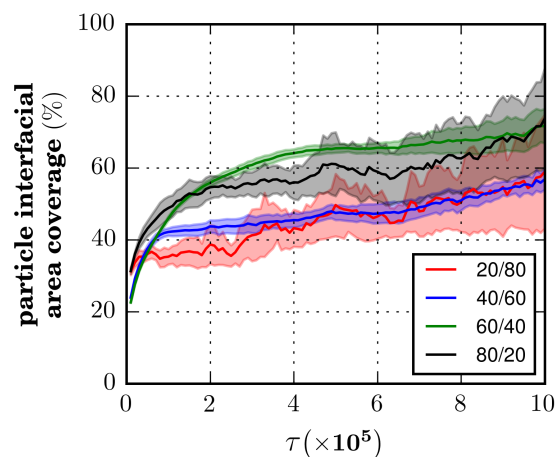


**Fig. 3** Percentage of interface covered by particles as a function of simulation time for thicker films. Legend indicates blend ratios.

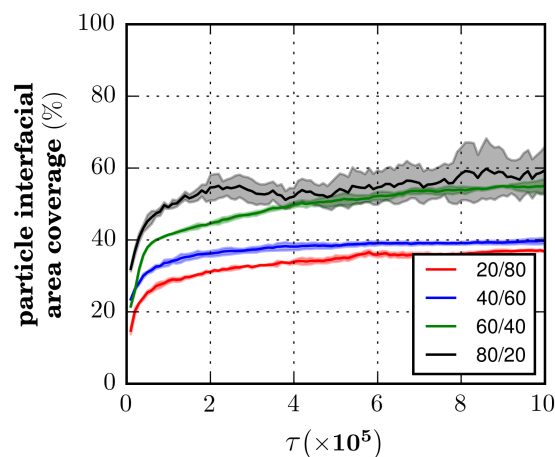


**Fig. 4** Percentage of interface covered by particles as a function of simulation time for thinner films. Legend indicates blend ratios.

Notice in Figures 3 and 4 that despite the spread in magnitude for the different blend ratios, the asymptotic behavior of all the films, both thick and thin, are all in the same general range of about 20-40% coverage. For a flat interface populated by particles with uniform size, the maximum percentage of interfacial area the particles can cover is equal to approximately

---

90.7% (i.e., close-packed structure). This happens when particles are packed as tightly as possible. The interfacial coverage percentage in our simulated bijel films is somewhat lower than this theoretical packing density for a number of reasons. First, the particles' Brownian motion and soft repulsive interactions never allows the particles to come into direct contact with one another. Second, the interface between the two liquid phases is never completely flat in the locality of an attached particle. Third, the particles themselves have variance in their size which frustrates close packing. Lastly, in many of the films, there is still interfacial area available that could accommodate more particles (especially in the tri-layer case).

### 1.3 Simulation Parameters

Table 1 lists all the simulation parameters and their numerical values. Although the mean particle radius  $\mu$  has a value of 4.0, the diffuse interfaces of the particles cause the effective particle radius to be larger than this (in our case by an increase of about 1 grid spacing  $\delta$ ). This effective particle radius is what is used to calculate the total volume fraction of particles

in the system.

**Table 1** CH/BD simulation parameters used in this study.

Parameter	Description	Value
$\delta$	xyz node spacing	1.0
$\Delta t$	time step	0.01
$M_i$	liquid phase mobilities	1.0
$\kappa$	interfacial energy par.	1.0
$w$	double well energy barrier par.	0.15
$\eta_i$	particle mobility	0.4
$\mu$	mean particle radius	4.0
$\sigma$	particle radius std.	1.5
$\beta_{max}$	wetting strength par.	5.0
$n_z$	number of nodes in the z-dir.	60 or 180

### References

- 1 M. Reeves, K. Stratford and J. H. J. Thijssen, *Soft Matter*, 2016, **12**, 4082–4092.